Serotonergic cortico-limbic and executive network dysfunction in Parkinson's disease impulse control disorders: a PET-fMRI study

Damiano Terenzi, Elise Metereau, Franck Lamberton, Hélène Klinger, Marine Huddlestone, Melinda de Oliveira, Jérôme Redoute, Léon Tremblay, Stéphane Thobois, Stéphane Prange

npj | parkinson's disease

Article

Published in partnership with the Parkinson's Foundation

https://doi.org/10.1038/s41531-026-01294-y

Serotonergic cortico-limbic and executive network dysfunction in Parkinson's disease impulse control disorders: a PET-fMRI study

Damiano Terenzi[1,2,3,9] ✉, Elise Metereau[1,2,9], Franck Lamberton[4,5], Hélène Klinger[2,6], Marine Huddlestone[2], Melinda De Oliveira[2], Jérôme Redoute[1,4], Léon Tremblay[7], Stéphane Thobois[1,2,8] & Stéphane Prange[1,2,8] ✉

Impulse control disorders (ICDs) affect up to 45% of Parkinson's disease (PD) patients, yet their neural mechanisms remain unclear. Using multimodal PET and resting-state fMRI in 23 PD patients (11 PDICD + , 12 PD-ICD-) and 14 healthy controls, we identified specific brain pathways underlying ICDs. PDICD+ patients showed steeper delay discounting and altered functional connectivity, including enhanced posterior parietal coupling within executive networks and disrupted salience–executive interactions. Critically, aberrant right supplementary motor area–amygdala connectivity was linked to ICD severity and decisional impulsivity. Path analysis revealed that increased SMA 5-HT_{2a} receptor availability was associated with enhanced SMA–amygdala coupling, which in turn was positively associated with ICD symptoms. By linking serotonergic dysfunction to disrupted motor-limbic networks and impulsive behavior, this study identifies targetable pathways for managing a common non-motor complication of PD.

Impulse control disorders (ICDs), including hypersexuality, binge eating, compulsive shopping, and gambling, are debilitating conditions characterized by impaired behavioral inhibition, causing substantial distress for patients and their families[1,2]. ICDs are particularly common in Parkinson's disease (PD), affecting up to 45% of patients within five years of diagnosis[3]. Their development is strongly linked to dopaminergic therapy, especially prolonged dopamine agonist use[3]. At present, no specific treatment exists, and management typically relies on reducing or discontinuing dopaminergic medication[4–6]. However, this strategy may trigger withdrawal symptoms, resulting in increased motor severity and non-motor symptoms like apathy and anxiety[5,7]. As a result, individualized, stepwise management is recommended[5]. This approach should address risk factors and comorbid psychiatric conditions (e.g., anxiety and depression)[1,8,9] and social consequences of ICDs[5,10].

Several clinical and demographic factors are known to increase vulnerability to ICDs in PD. Younger age at PD onset, male sex, a personal or family history of addictive or impulsive behaviors, and higher novelty-seeking or impulsivity traits have all been associated with greater ICD risk[1,11,12]. Dopamine agonist therapy remains the strongest modifiable risk factor, consistent with its potentiating effects on mesocorticolimbic reward circuits[5,13–15]. Psychiatric comorbidities—including anxiety, depression, and sleep disturbances—further contribute to susceptibility[16,17]. In contrast, genetic contributions to ICDs in PD remain poorly understood. Although variants in dopaminergic, serotonergic, and opioid-system genes have been investigated, findings to date have been inconsistent[12,18,19]. This gap highlights the need for integrative approaches that combine clinical phenotyping with neuroimaging to better characterize vulnerability to ICDs in PD[20,21].

[1]Univ Lyon, Lyon Neuroscience Research Center (CRNL), CNRS UMR 5292, INSERM U1028, Bron, France. [2]Hospices Civils de Lyon, Hôpital Neurologique Pierre Wertheimer, Service de Neurologie C, Centre Expert Parkinson NS-PARK/FCRIN network, Bron, France. [3]Emotions, Neurocognition and Therapeutic Behavioral Approaches (ENACT) Team, University of Nîmes, Nîmes, France. [4]CERMEP-Imaging platform, Groupement Hospitalier Est, Bron, France. [5]Univ Lyon, SFR Lyon-Est, CNRS UAR 3453, INSERM US7, Lyon, France. [6]Hospices Civils de Lyon, Hôpital Neurologique Pierre Wertheimer, Neurological Intensive Care Unit, Bron, France. [7]Centre de Neurosciences Cognitives-UMR 5229, CNRS-Université de Lyon 1, Bron, France. [8]Univ Lyon, Université Claude Bernard Lyon 1, Faculté de Médecine et de Maïeutique Lyon Sud Charles Mérieux, Oullins, France. [9]These authors contributed equally: Damiano Terenzi, Elise Metereau. ✉e-mail: damiano.terenzi@inserm.fr; stephane.prange@chu-lyon.fr

Evidence from functional and morphometric imaging studies indicates dysfunction within the meso-corticolimbic–striatal circuit in PD patients with ICDs[15]. Alterations have been observed across cortical and subcortical regions crucial for reward processing, including the anterior cingulate cortex (ACC), orbitofrontal cortex (OFC), insula, and ventral striatum (VS)[22–25].

Moreover, molecular imaging studies support the role of a hyperdopaminergic state in PD patients with ICDs, characterized, notably, by increased dopamine release in the VS in response to reward-related stimuli[1,23,26,27].

More recently, serotonergic dysfunction has also been implicated in ICDs in PD. Using 11C-DASB and ^{18}F-altanserin PET, PD patients with ICDs were found to have more preserved presynaptic SERT availability in the left posterior putamen. They also showed increased 5-HT_{2a} receptor availability in the bilateral supplementary motor area (SMA), precentral gyrus, and right dlPFC. This highlights a key role of serotonergic modulation in motor and associative circuits in PD-ICD[28].

Despite these advances, the mechanisms underlying ICDs remain unclear, particularly regarding how the interplay of limbic and motor circuits relates to distinct impulsivity domains. These domains are assessed using behavioral tasks, including delay discounting, Go/No-Go, Stop-Signal, and risk-taking tasks. However, divergent results across studies continue to challenge our understanding on the contribution of specific cortical and subcortical regions to ICD pathogenesis[15,29]. They also raise questions about how these regions integrate within large-scale brain networks. This network-based perspective shifts focus from regional abnormalities to broader connectivity patterns that may more accurately reflect the distributed nature of cognitive and behavioral control[30–34].

Resting-state functional magnetic resonance imaging (rs-fMRI) provides a valuable tool for probing intrinsic brain function and connectivity patterns[35–37]. In PD patients with ICDs, rs-fMRI studies have suggested connectivity alterations between the striatum and cortical regions[38–40], as well as an imbalance between large-scale networks, such as the salience network (SN), the Default Mode Network (DMN), and the central executive network (CEN)[25,38,39,41]. In particular, the SN, anchored by the anterior insula (AI), ACC, rostral prefrontal cortex (RPFC), and superior marginal gyrus (SMG)[42,43], is critical for detecting behaviorally relevant stimuli. Aberrant SN functioning may bias attentional resources toward reward-related cues at the expense of goal-directed behaviors. This shift may contribute to heightened impulsivity and compulsive behaviors[38,41]. In contrast, the CEN, encompassing dorsolateral prefrontal cortex (dlPFC) and posterior parietal cortex (PPC)[42,43], subserves cognitive control and working memory processes essential for inhibiting inappropriate responses[15,38,44].

The PPC consists of multiple subregions with distinct functional network affiliations. In the CONN toolbox Network Atlas[42], the PPC parcel is assigned to the frontoparietal/central executive network. However, other parcellations classify ventral/lateral PPC regions—such as the angular gyrus—as part of the DMN[45]. Recent connectivity-based atlases further highlight this heterogeneity within the PPC[46–49].

The DMN supports self-referential processing, which in PD-ICD patients may manifest as greater focus on internal impulses and thoughts[38,39,44]. Contributing to both the CEN and DMN, PPC engagement may influence the balance between internally and externally directed processes, shaping the neural context for ICD vulnerability in PD.

However, it remains largely unknown how monoaminergic systems modulates large-scale network dynamics, and contribute to behavioral inhibition or the lack thereof in PD-ICD[29]. In particular, how serotonergic changes alter network dynamics is unknown. These alterations may modulate impulsivity and contribute to ICDs. Therefore, we performed a multimodal PET-resting state fMRI study. We aimed to investigate whether resting-state functional connectivity within and between the CEN and SN differs in PD patients with ICDs, PD patients without ICDs, and healthy controls. We also investigated whether these networks are associated with serotonergic circuits. Prior work shows that ICDs in PD are linked to various forms of impulsivity, with abnormalities in delay discounting (decisional impulsivity) more consistently reported than deficits in motor or waiting impulsivity[6,28,50–52]. Based on this, we predicted that PD patients with ICDs may exhibit steeper delay discounting. We also hypothesized that PD patients with ICDs would show increased 5-HT_{2a} receptor availability in the SMA, precentral gyrus, and dlPFC. These regions, key nodes of sensorimotor and associative networks involved in behavioral inhibition, may show compensatory resting-state connectivity with regions of the salience, limbic, and frontostriatal control networks. We further anticipated that the strength of these connectivity patterns would relate to both regional serotonergic alterations (PET) and clinical measures, including ICD severity and decisional impulsivity. By combining PET and rs-fMRI, this multimodal approach aims to delineate how molecular abnormalities in specific brain areas are associated with large-scale network dysfunction and the severity of ICDs in PD.

Results

Demographic, clinical and behavioral Characteristics

Kruskal–Wallis tests were performed to assess differences between groups (HC, PDICD −, PDICD +) across behavioral tasks. No significant group effects were found for SSRT in the SST task or premature responses in the 4-CSRT task (see Supplementary Materials).

A significant group effect was observed for log factor k in the Kirby delay discounting questionnaire ($\chi^2(2) = 7.29$, $p = 0.026$). Pairwise Wilcoxon rank-sum tests with Benjamini–Hochberg correction showed that PDICD+ individuals had significantly lower log factor k values than PDICD − participants ($W = 24.5$, $p = 0.034$), suggesting steeper discounting in the PDICD+ group. No significant differences were observed between HC and PDICD− ($p = 0.299$) or between HC and PDICD+ ($p = 0.103$) (see Fig. 1 and Supplementary Materials for detailed statistics). Further analyses examining delay discounting across reward magnitudes (small, medium, and large) showed that PDICD+ individuals exhibited significantly more impulsive choice behavior than PDICD-, particularly for medium ($W = 23.0$, $p = 0.037$) and large ($W = 23.0$, $p = 0.023$) delayed rewards, reflecting a stronger preference for smaller immediate rewards in these conditions (see Table S3, Supplementary Materials). No other significant group differences emerged (all Ps > 0.058).

ROI-to-ROI analysis

PDICD+ showed significantly higher rsFC than PDICD− between the left and right PPC, two regions that are part of the CEN and the DMN ($t(31) = 2.76$, pFDR = 0.027; Fig. 2a). Notably, no significant differences in rsFC were observed between PDICD+ and HC.

In contrast, comparison between PDICD− and HC revealed decreased rsFC in three clusters: left and right SMG ($t(32) = -3.56$, pFDR = 0.024), right insula – right ACC ($t(32) = -3.27$, pFDR = 0.027), and left insula – right SMG ($t(32) = -2.98$, pFDR = 0.046) (See Fig. S1, Supplementary Materials).

Seed-to-voxel analysis

A seed-to-voxel analysis was conducted using a voxel-wise threshold of $p < 0.005$ (uncorrected) and a cluster-level threshold of $p < 0.05$ (FDR-corrected), as implemented in CONN. Using the right SMG from the SN as seed revealed significantly higher connectivity in PDICD+ compared to PDICD− with a cluster centered in the left striatum, peaking in the left putamen and extending into the left caudate ($t(31) = 4.85$, pFDR = 0.0469, peak coordinate: −18, −8, +6, k = 432). No other significant group differences were found with other salience or CEN seeds (see Supplementary Results for comparisons between PDICD+ and HC, as well as between PDICD− and HC).

Moreover, using the right SMA as seed—a region implicated in ICD in PD and modulated by the serotonergic system[28,29,53]—PDICD+ showed increased rsFC with the right amygdala ($t(31) = 5.04$, pFDR = 0.0226, peak coordinate: +34, −2, −18, k = 488) (Fig. 3a). No other significant effects were observed when using additional seeds previously associated with serotonergic dysfunction in ICD in PD, such as the precentral gyrus and the right dorsolateral prefrontal cortex.

Correlation and Structural Equation Modeling analyses

We found that lower rsFC within the right and left PPC of the CEN network was associated with more severe ICD scores in the PDICD+ group (rho =

-0.77, $p = 0.0006$) but not in the PDICD- ($p = 0.1320$) (Fig. 2b). Furthermore, across PD patients, higher QUIP scores were positively correlated with increased rsFC between the right SMG (seed) and the left putamen (rho = 0.52, $p = 0.010$), as revealed by the seed-to-voxel analysis.

Importantly, rsFC between the right SMA (seed) and right amygdala was positively associated with QUIP scores (r = 0.66, $p = 0.0005$) and log k (r = 0.43, $p = 0.0388$) (Fig. 3b, c), reflecting greater ICD severity and increased delay discounting, respectively. Moreover, ^{18}F-Altanserin binding in the right SMA was positively correlated with right SMA–right amygdala rsFC (r = 0.47, p = 0.0223), indicating that higher serotonergic receptor availability in the right SMA is linked to stronger functional connectivity between this region and the right amygdala. Moreover, ^{18}F-Altanserin binding in the right SMA showed a positive association with QUIP scores (r = 0.53, $p = 0.0087$).

To further characterize these relationships, we conducted two different SEM. ^{18}F-Altanserin binding in the right SMA and right SMA-amygdala rs-FC were significantly correlated ($p = 0.040$). In the path analysis examining associations with delay discounting of rewards (log k), ^{18}F-Altanserin binding in the right SMA was not associated with discounting (p = 0.830), whereas right SMA-amygdala rs-FC was positively associated with discounting ($p = 0.020$); delay discounting was not significantly associated with QUIP-RS (p = 0.158). ^{18}F-Altanserin binding in the right SMA showed a marginal positive effect on QUIP-RS (p = 0.068), and right SMA-amygdala rs-FC was positively associated with QUIP-RS ($p = 0.018$). The model explained 21.9% of the variance in delay discounting and 54.3% in QUIP-RS (see Fig. 4a).

In the parallel model including UPPS scores, neither ^{18}F-Altanserin in the right SMA (β = 0.268, p = 0.244) nor connectivity (β = -0.125, $p = 0.588$) were significantly associated with impulsivity as measured through UPPS. Also, UPPS scores were positively associated with QUIP-RS (β = 0.345, $p = 0.009$), and right SMA-amygdala rs-FC was also positively associated with QUIP-RS (β = 0.573, $p < 0.001$), whereas ^{18}F-Altanserin did not (β = 0.190, $p = 0.208$). The model accounted for 5.6% of the variance in UPPS scores and 61.6% in QUIP-RS scores. See Fig. 4b.

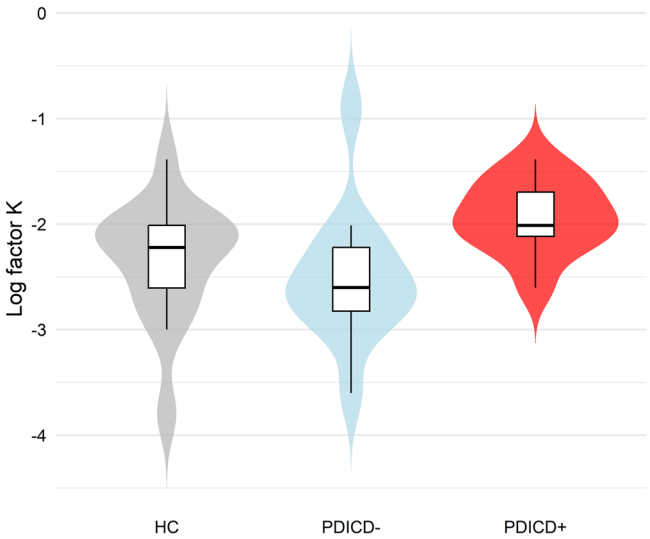

Fig. 1 | Delay discounting task. Violin plots illustrate the distribution and density of log-transformed factor k across healthy controls (HC, gray), Parkinson's disease patients without impulse control disorders (PDICD − , blue), and patients with impulse control disorders (PDICD + , red). PDICD+ showed steeper delay discounting than PDICD− participants ($p = 0.034$).

Structural and diffusion MRI analysis

No significant differences in gray matter volume, cortical thickness, sulcus depth, fractional anisotropy, or mean diffusivity were observed between PDICD+ and PDICD− groups at the threshold-free cluster enhancement family-wise error corrected threshold (p-TFCE-FWE < 0.05, see supplementary materials for further details).

Discussion

In PD patients with ICDs, we demonstrate that dysfunction of large-scale network dynamics between the SN and CEN subserve the clinical expression of ICD related to impaired behavioral inhibition and are modulated by the serotonergic system by cortical 5HT2A-receptor availability highlighting its role on motor to limbic inhibition networks.

PD-ICD+ patients had heightened decisional impulsivity, reflected by steeper delay discounting. This finding is in line with previous studies reporting greater decisional impulsivity in PDICD+ for both secondary rewards such as money[6,21,28,50–52] and primary rewards such as food[6] and erotic stimuli[54]. We also examined other facets of impulsivity but found no differences between the three groups of participants in motor impulsivity (SST) or waiting impulsivity (4-CSRT). Together, this pattern suggests that impulsivity in PDICD+ is specifically linked to reward-based decision-making rather than deficits in motor inhibition or waiting control. These results reinforce the view that impulsivity is multifaceted and supported by

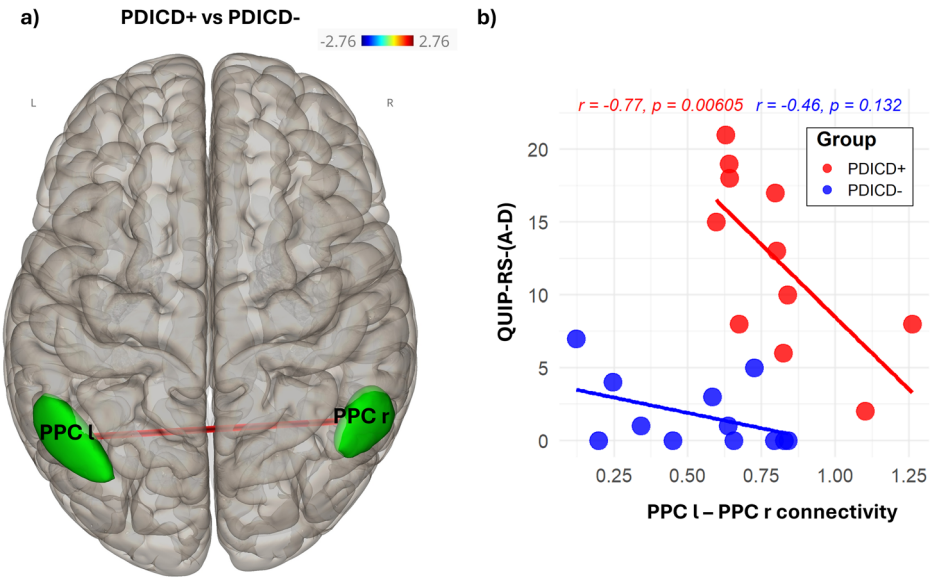

Fig. 2 | ROI-to-ROI functional connectivity differences between PDICD+ and PDICD− groups. **a** 3D brain rendering showing regions of interest (ROIs) within the central executive network (CEN) with significant between-group differences. PDICD + participants exhibited higher left-right PPC connectivity (pFDR = 0.027). **b** Scatterplot showing Fisher r-to-z transformed connectivity values. Higher bilateral PPC connectivity correlated with greater QUIP-RS scores in PDICD+ (r = 0.77, $p = 0.006$) but not PDICD− participants. Statistical significance was assessed using connection-level $p < 0.05$ with FDR correction at cluster level (pFDR < 0.05).

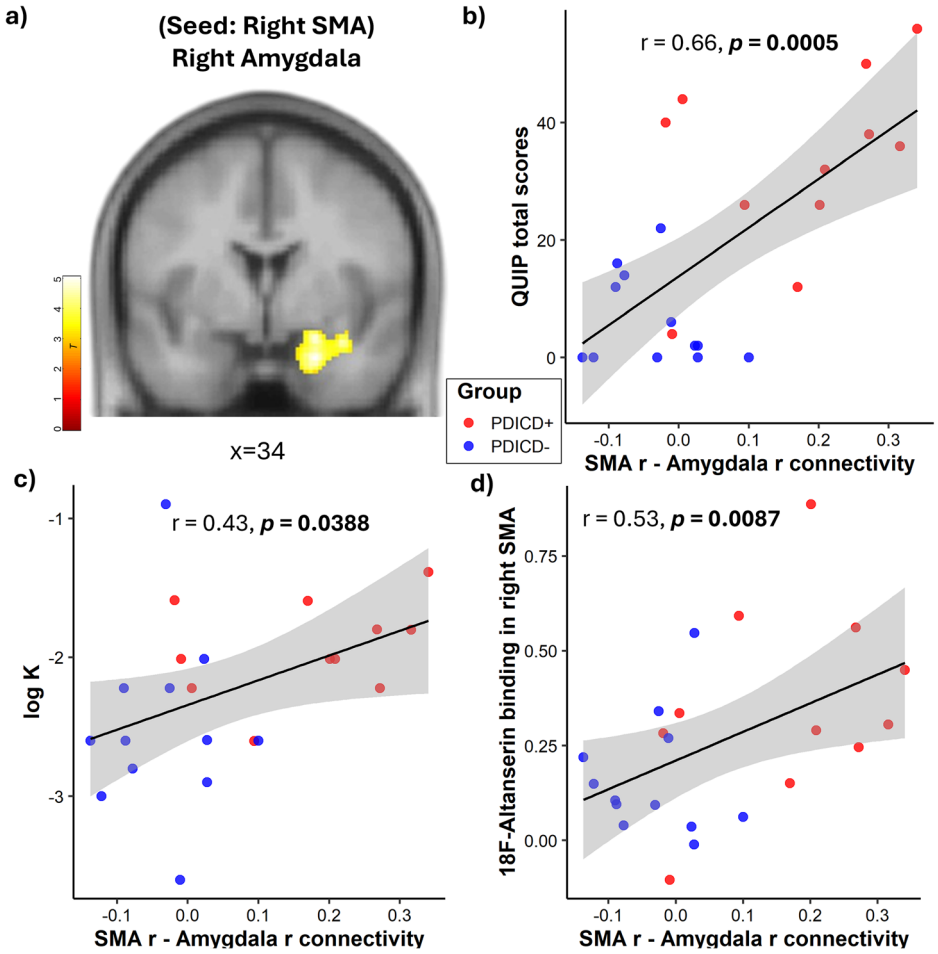

Fig. 3 | Seed-based functional connectivity analysis using right supplementary motor area (SMA). **a** Statistical map showing increased resting-state functional connectivity between right SMA (seed region) and right amygdala in PDICD+ compared to PDICD− participants ($t(31) = 5.04$, pFDR = 0.0226). **b**, **c** Scatterplots show Fisher r-to-z transformed connectivity values across all PD patients. **b** Right SMA-amygdala connectivity positively correlated with QUIP total scores ($r = 0.66$, $p = 0.0005$). **c** Right SMA-amygdala connectivity positively correlated with log-transformed K values ($r = 0.43$, $p = 0.0388$). **d** Right SMA-amygdala connectivity positively correlated with ^{18}F-Altanserin binding in the right SMA ($r = 0.53$, $p = 0.0087$). Statistical maps were thresholded at voxel-wise $p < 0.005$ (uncorrected), followed by cluster-level FDR correction. Red dots indicate PDICD+ participants; blue dots indicate PDICD− participants.

distinct neural mechanisms[21,29,55,56], with ICD in PD primarily associated with decisional impulsivity[6,13,28,50–52].

At the neural level, PD-ICD+ patients showed increased rsFC within the CEN, specifically between the left and right PPC, suggesting enhanced PPC integration in a network subserving executive control and proactive inhibitory processes. As the PPC is also a key hub of the DMN, this effect may additionally point to cross-network dynamics whereby regions implicated in self-referential processing and greater focus on internal impulses become engaged in control-related functions. One possible interpretation is that this increased connectivity reflects a compensatory attempt to upregulate executive and proactive inhibitory mechanisms; alternatively, the very same control systems could also be implicated in processes that favor the emergence of ICDs. This aligns with previous reports of CEN involvement, including parietal regions linked to inhibitory control deficits in PD-ICD.

The functional significance of these connectivity patterns is supported by their relationship to clinical symptoms. Higher bilateral PPC connectivity was associated with lower ICDs severity in PDICD +, suggesting a compensatory role of bilateral PPC connectivity within the CEN.

In addition to the ROI-to-ROI analysis, we performed a complementary seed-to-voxel analysis using the same predefined ROIs to examine whole-brain connectivity. The right SMG (part of the SN) showed significantly higher connectivity with the left striatum (peaking in the putamen and extending into the caudate) in PDICD+ compared to PDICD −. Given the VS central role in reward processing and impulse control[57] and the involvement of the SMG in salience detection and attentional reorienting[58,59], this enhanced coupling may reflect aberrant salience attribution to reward-related cues, contributing to impulsive behaviors in ICD[14,60]. The role of caudate in ICD vulnerability is further supported by findings of serotonergic dysfunction in this region correlating with increased urgency and choice impulsivity in PD patients[28,29].

Building on previous PET findings from our group[28] showing increased cortical ^{18}F-altanserin binding in PDICD+ patients—particularly in the SMA, precentral gyrus, and right dlPFC, regions critical for behavioral inhibition[6,28,61]—we conducted seed-to-voxel analyses of resting-state functional connectivity using these regions as separate ROIs.

The right SMA, a central node of the sensorimotor network[28,29], demonstrated increased connectivity with the right amygdala (compared with PDICD-). Importantly, this SMA–amygdala coupling showed strong positive associations with both QUIP-RS scores and delay discounting measures across PD patients, directly linking enhanced connectivity to ICD severity and impulsive decision-making. These findings suggest that aberrant integration between motor planning circuits (SMA) and emotional valuation systems (amygdala)[62,63] may amplify reactivity to reward-related stimuli, thereby contributing to the pathophysiology of ICD in PD.

Notably, despite the altered SMA–amygdala connectivity pattern, PDICD+ patients exhibited intact basic motor inhibition performance on the SST. This dissociation indicates that the contribution of SMA to ICD pathology likely involves emotional-inhibitory control integration and action selection within reward contexts, rather than motor stopping mechanisms. The preserved motor inhibition alongside dysregulated emotional-inhibition coupling supports a model where ICD emerges from specific disrupted integration between motivational and inhibitory control systems rather than global inhibitory deficits.

A key strength of our study lies in the multimodal integration of PET and fMRI, which offers novel mechanistic insight into ICD in PD. We observed a positive association between ^{18}F-altanserin binding in the right SMA and right SMA–amygdala rsFC, indicating that higher serotonergic

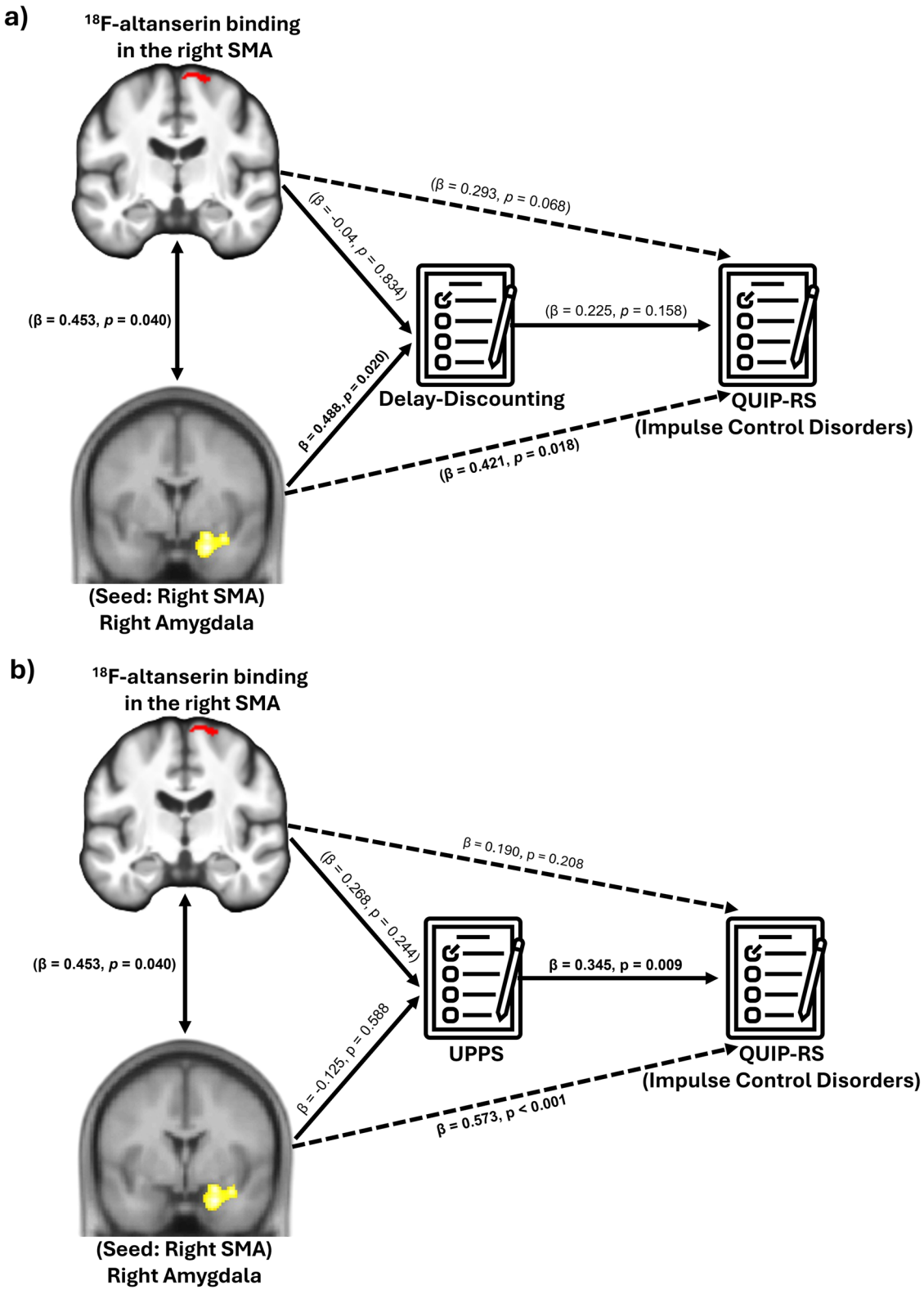

Fig. 4 | Path analysis of serotonergic binding, functional connectivity, impulsivity (decisional and trait impulsivity) and QUIP-RS scores. a ^{18}F-Altanserin binding in the right SMA and right SMA-amygdala functional connectivity were significantly correlated ($p = 0.040$). In the delay discounting model, connectivity was positively associated with discounting (log k) ($p = 0.020$), whereas ^{18}F-Altanserin binding in the right SMA did not ($p = 0.830$); connectivity and marginally^{18}-Altanserin binding were positively associated with QUIP-RS ($p = 0.018$ and $p = 0.063$). **b** In the UPPS model, UPPS scores and connectivity were positively associated with QUIP-RS ($p = 0.009$ and $p < 0.001$), whereas^{18}-Altanserin binding and connectivity were not associated with impulsivity ($p = 0.244$ and $p = 0.588$).

receptor availability in SMA relates to stronger coupling with a limbic structure critically involved in emotional regulation[64,65]. Crucially, SEM analysis revealed that ^{18}F-Altanserin binding in the right SMA was associated with right SMA–amygdala rs-FC, and this connectivity was associated with both steeper delay discounting and higher QUIP-RS scores. Although PDICD+ patients displayed steeper delay discounting compared to PDICD-, this behavioral measure was not associated with ICD severity within the SEM framework, suggesting that the expression of ICDs in PD may depend more on the underlying SMA–amygdala circuitry than on overt measures of decisional impulsivity. In addition, trait impulsivity, as measured by UPPS scores, was associated with ICD severity independently, pointing to a complementary psychological construct contributing to ICDs.

Overall, our findings highlight a novel pathway linking serotonergic dysfunction, aberrant cortico-limbic connectivity, and the behavioral phenotype of ICD. Specifically, compromised serotonergic signaling in SMA—an area bridging control of inhibition and emotion regulation[62,63,66]—may bias its interactions with the amygdala, amplifying impulsive tendencies and maladaptive reward sensitivity. By directly linking molecular, network-level, behavioral, and personality trait measures, our results provide a new framework for understanding the neurobiological basis of ICD in PD.

Interestingly, no significant structural differences in gray matter volume, cortical thickness, or white matter integrity were observed between PDICD+ and PDICD− groups. These findings suggest that functional connectivity alterations in ICDs may occur independently of gross structural changes. Despite providing novel insights into the neural and behavioral mechanisms underlying ICD in PD, several limitations should be considered. First, we cannot exclude that patients with single or multiple ICDs of different types may have different pathophysiological underpinnings. Second, the sample size, particularly for the PDICD+ group, was modest, which may limit statistical power and the broader generalizability of the findings. In particular, the small sample size and the cross-sectional design preclude any causal inference. The limited sample size also increases the risk of overfitting in our SEM analysis and larger, longitudinal samples are required to further validate these associations. Moreover, future longitudinal studies will be important to clarify whether these neural patterns represent predisposing factors or adaptive changes associated with ICD. Third, although ICDs can strongly affect quality of life in patients with PD, neuroimaging is not currently established for routine screening or prevention. PD diagnosis remains primarily clinical, and neuroimaging is typically used to exclude atypical or secondary parkinsonism. Nevertheless, the functional connectivity patterns identified here advance our understanding of the neural correlates of ICD in PD. Accordingly, functional imaging may inform risk stratification alongside clinical assessment in high-risk patients. However, this requires further longitudinal studies to be validated as a clinical tool.

Altogether, this study provides insights into the neural and molecular underpinnings of ICDs in PD, showing that heightened decisional impulsivity and maladaptive reward processing are associated with specific neural and molecular alterations. PDICD+ patients show increased executive network connectivity, disrupted salience–executive interactions, and aberrant SMA–amygdala coupling linked to serotonergic dysfunction and ICD severity. Crucially, these changes reflect specific impairments in emotional–inhibitory control integration rather than global inhibition deficits, pinpointing a targeted neural substrate for impulsive behavior. By bridging molecular, network, and behavioral levels, our findings provide a unified framework for understanding ICDs and highlight precise neural circuits as potential targets for therapeutic intervention.

Methods

Patients

A total of twenty-three patients diagnosed with PD based on the Movement Disorder Society's criteria were recruited from the Pierre Wertheimer Lyon University Neurological Hospital. The study included eleven PD patients exhibiting ICD (PDICD +) and twelve PD patients without ICD (PDICD −), matched for age, gender, and duration of disease. Additionally, fourteen healthy individuals, also matched for age and gender, served as control participants (HC). All participants underwent evaluation by a neuropsychologist experienced in PD, using a structured and standardized interview such as the Ardouin Scale of Behavior in PD (ASBPD)[67] (see Table 1).

Patients were classified as ICD positive if they had a score of ≥2 for at least one of the following behaviors at the time of the study or within the previous two years: pathological gambling, compulsive sexual behavior, binge eating, or compulsive shopping. In contrast, individuals in the PDICD − and HC groups were required to have no history of any ICD (a score of 0 on the ASBPD for gambling, shopping, eating, and hypersexuality) and no signs of hyperdopaminergic behavior with significant consequences (ASBPD score ≤1 for items such as creativity, eating habits, hobbyism, punding, risk-taking, or dopaminergic misuse). Accordingly, patients with remote (>2 years) history for ICDs were not eligible for all groups including the PDICD− group and were therefore excluded for this study.

Participants were excluded if they showed signs of cognitive impairment, defined as a Montreal Cognitive Assessment (MoCA) score ≤24 or a Frontal Assessment Battery (FAB) score ≤14. Other exclusion criteria included substance abuse, recreational drug use, or use of psychotropic medications within the preceding three months. Individuals with contraindications to PET or MRI imaging or those experiencing severe resting tremor or dyskinesia were also excluded. The study received approval from the French national ethics committee and the drug regulatory agency (ANSM), and it was in accordance with the declaration of Helsinki. The study was registered as a clinical trial (NCT03970239 || https://www.clinicaltrials.gov/study/NCT03970239?a=12019-05-06). Written informed consent was obtained from all participants.

Demographic, clinical and neuropsychological assessment

Demographic data were collected for each participant, including age, sex, and duration of PD. The severity of both motor and non-motor symptoms of PD was evaluated in the on-medication state using the Movement Disorder Society–Revised Unified PD Rating Scale (MDS-UPDRS)[68]. A comprehensive neuropsychological assessment was conducted to evaluate several dimensions: the severity of ICDs was assessed using the Questionnaire for Impulsive-Compulsive Disorders in PD–Rating Scale (QUIP-RS)[69]. Impulsivity traits were measured using the Urgency, Premeditation, Perseverance, Sensation Seeking, and Positive Urgency Impulsive Behavior Scale (UPPS-P)[70]; Additional assessments addressed comorbid neuropsychiatric symptoms: apathy was measured using the Starkstein Apathy Scale[71,72]; trait anxiety was evaluated with the State-Trait Anxiety Inventory, part B (STAI-Yb)[73]; and depressive symptoms were assessed using the Beck Depression Inventory, Second Edition (BDI-2)[74]. All participants also completed the REM Sleep Behavior Disorder Screening Questionnaire (RBDSQ)[75]. See Table 1.

Impulsivity Assessment

To assess different facets of impulsivity, we used the four-factor UPPS questionnaire along with a set of behavioral tasks[55]. Specifically, we examined both decisional and motor impulsivity. Decisional impulsivity was evaluated by measuring the ability to delay future monetary rewards using the Monetary Choice Questionnaire[76]. Motor impulsivity was assessed through the Stop Signal Task (SST), which measures the capacity to inhibit ongoing actions[77,78], and the human four-choice serial reaction time task (4-CSRT), which evaluates waiting impulsivity by quantifying the ability to withhold premature responses[79]. The main outcome measures were stop signal reaction time (SSRT) for the SST, the log of factor k for the Monetary Choice Questionnaire, and the number of premature responses for the 4-CSRT. SSRT in the SST were calculated using the integration method as described in ref. 77. Accordingly, for each participant, the distribution of reaction times on correct go trials was used to determine the reaction time corresponding to the percentile equal to the probability of responding on stop trials. The SSRT was then estimated by subtracting the participant's mean stop-signal delay (SSD) from this reaction time. Go omission trials

Table 1 | Demographic and clinical data of PD patients and HC

Variable	HC (n = 14)	PDICD- (n = 12)	PDICD+ (n = 11)	Main group effect
Age	60.07 (8.76)	59.33 (9.87)	58.45 (11.94)	P = 0.9901[a]
Sex, male	11 (79%)	11 (92%)	9 (82%)	P = 0.7442[b]
BMI	25.41 (3.83)	23.30 (2.52)	27.36 (4.18)	**P = 0.0198**[a]
Time since diagnosis, years	-	6.42 (4.10)	6.45 (5.39)	P = 0.8044[c]
LEDD total, mg	-	976.71 (641.47)	916.86 (468.34)	P = 0.8801[c]
LEDD, levodopa, mg	-	718.48 (578.20)	711.23 (388.85)	P = 0.9013[c]
LEDD, DA, mg	-	208.23 (130.16)	114.73 (120.40)	P = 0.0630[c]
MDS UPDRS I score	-	4.67 (3.42)	9.73 (2.94)	**P = 0.0022**[c]
MDS UPDRS II score	-	6.33 (4.52)	7.73 (4.34)	P = 0.4393[c]
MDS UPDRS III score	-	21.83 (11.19)	27.82 (14.63)	P = 0.4051[c]
MDS UPDRS IV score	-	3.17 (3.04)	3.00 (2.79)	P = 0.9491[c]
Hoen and Yahr	-	1.75 (0.62)	1.73 (0.65)	P = 0.9628[c]
QUIP-RS total score	4.29 (5.20)	6.17 (7.79)	33.09 (15.50)	**P = 0.0001**[a]
QUIP-RS A-D subscore	1.71 (2.61)	1.75 (2.42)	12.45 (6.09)	**P < 0.0001**[a]
ASBPD hypodopaminergic	1.08 (1.16)	0.93 (1.0)	4.18 (2.82)	**P = 0.0013**[a]
ASBPD hyperdopaminergic	0.29 (0.83)	1.92 (1.38)	7.18 (5.19)	**P < 0.0001**[a]
MoCA score	28.93 (1.44)	28.67 (0.98)	28.82 (0.75)	P = 0.5123[a]
BREF score	17.43 (0.65)	17.33 (0.89)	17.09 (0.94)	P = 0.6447[a]
Starkstein score	6.57 (2.82)	6.75 (4.18)	9.82 (6.15)	P = 0.5450[a]
BDI-2 score	3.57 (2.93)	2.25 (1.86)	9.00 (6.87)	**P = 0.0021**[a]
STAI-Yb score	34.36 (6.64)	30.33 (7.77)	38.91 (6.93)	**P = 0.0415**[a]
RBDSQ	2.64 (1.91)	4.67 (4.05)	4.45 (3.45)	P = 0.4121[a]
UPPS premeditation	19.71 (5.43)	17.92 (3.06)	20.45 (8.63)	P = 0.7768[a]
UPPS perseverance	16.79 (2.29)	16.33 (4.29)	17.73 (4.88)	P = 0.6320[a]
UPPS sensation	27.57 (8.72)	25.08 (7.75)	25.27 (7.98)	P = 0.7704[a]
UPPS urgency	24.79 (4.44)	20.00 (5.70)	27.27 (6.23)	**P = 0.0300**[a]
UPPS Total	88.86(13.74)	79.33 (13.89)	90.73 (15.64)	P = 0.1552[a]

Continuous variables are reported as mean (standard deviation). Categorical variables are presented with frequency (percentage). Bold values indicate statistical significance at $P < 0.05$.
ASBPD ardouin scale of behaviors in Parkinson's disease, *BMI* body mass index, *LEDD* levodopa equivalent daily dose, *DA* dopaminergic agonist, *HC* healthy controls, *ICD* impulse control disorders, *MDS-UPDRS* movement disorder society unified Parkinson's disease rating scale, *MoCA* Montreal cognitive assessment, *PD* Parkinson's disease, *QUIP-RS* questionnaire for impulsive-compulsive disorders in Parkinson's disease–rating scale, *RBDSQ* REM Sleep Behavior Disorder Screening Questionnaire, *BDI* Beck depression inventory, *STAI* state-trait anxiety inventory, *UPPS* urgency, premeditation, perseverance, sensation seeking, positive urgency impulsive behavior scale
[a]Main effect of group (HC, PDICD −, PDICD +) *P*-values are calculated with the Kruskal–Wallis test.
[b]Group effects on categorical variables are calculated with Fisher's exact test.
[c]Main effect of ICD in Parkinson (PDICD −, PDICD +) *P*-values are calculated with the Wilcoxon rank-sum test.

were excluded from the analysis, in line with standard practice. This procedure provides an estimate of the time required for successful response inhibition.

Scanning procedure

All MRIs were acquired on a MAGNETOM Prisma 3 T scanner (Siemens Healthcare, Erlangen, Germany). High resolution anatomical images (T1-weighted MP-RAGE with vNav based prospective motion correction[80]) were acquired with repetition time (TR) = 3000 ms, echo time (TE) = 2.98 ms, flip angle = 8°, field of view (FOV) = 224 × 256 mm, voxel size 1 × 1 × 1 mm^3, 176 sagittal slices with slice thickness = 1 mm and in-plane acceleration with GRAPPA factor of 2.

Rs-fMRI echo-planar images were acquired for 10 min (400 volumes) with TR = 1500 ms, TE = 33.6 ms, flip angle = 60°, FOV = 20.8 × 20.8 mm, 64 axial slices and voxel size 2.3 × 2.3 × 2.3 mm^3 and slice acceleration with MultiBand factor of 4. Subjects were instructed to rest quietly, to keep their eyes open and not to fall asleep.

Diffusion-weighted images were acquired in 62 directions for two shells (b = 1000 s/mm^2 and b = 2000 s/mm^2 using bipolar gradients) with TR = 5500 ms, TE = 85 ms, flip angle = 90°, field of view (FOV) = 220 mm, voxel size 2 × 2 × 2 mm^3, and slice acceleration with MultiBand factor of 2, along with 16 null diffusion-weighted volumes (b = 0 s/mm^2).

The participants in this study also underwent PET scans as previously described in Prange et al.[28]. In particular, they underwent PET acquisition with 18F-altanserin using a high-resolution PET scanner Biograph mCT/S 64. The tracer was administered as a bolus of ~170 MBq (2.3 MBq/kg) followed by a continuous infusion up to 1.3 MBq/kg, applying a bolus-to-infusion ratio of 1.75 h. PET acquisition during steady state was performed for 40 min starting 2 h after administration and reconstructed into five 8-min frames. Data were corrected for attenuation and scatter and reconstructed with UltraHD TOF OSEM, yielding 256 × 256 × 109 volumes with 1.06 × 1.06 × 2.03 mm^3 voxels. Structural MRI was acquired using a 3 T system MAGNETOM Prisma with an MPRAGE sequence MPRAGE including volumetric navigators (vNav; TR = 3 s; 1 mm isotropic).

Binding potential estimation

Motion correction was applied by realigning individual frames to the subject-specific mean image using minc-tools. Cerebellar white matter (CWM), segmented from each T1-weighted MRI using MAPER, served as the reference region. Voxel-wise non-displaceable binding potential

(BPND) maps were computed using the steady-state formula: BPND = (CVOI − CCWM) / CCWM, where CVOI and CCWM denote steady-state mean radioactivity in the target and reference regions, respectively.

Statistical analysis

Group comparisons for categorical variables were conducted using Fisher's exact test, while continuous variables were analyzed using the Kruskal–Wallis test. Pairwise group differences were further examined with Wilcoxon's test, applying the Benjamini–Hochberg procedure to adjust for multiple comparisons. Relationships between neuropsychological measures and behavioral task outcomes were explored using Spearman or Pearson correlation coefficients, depending on data distribution. Normality of the data was evaluated with the Kolmogorov–Smirnov test. All statistical analyses were performed using R software.

All resting-state fMRI analyses were conducted using the CONN22 toolbox[42], running on MATLAB 2023b (The MathWorks Inc., Natick, MA, USA) and SPM12 (Wellcome Trust Center for Neuroimaging, London, UK). Preprocessing followed CONN's default pipeline for volume-based analyses with direct normalization to MNI space. This included functional realignment and unwarping, slice-timing correction, ART-based outlier detection (defined as framewise displacement > 0.3 mm or global BOLD signal deviation > 3 SD[81]), normalization of functional and anatomical images to MNI space, and tissue segmentation into gray matter, white matter, and cerebrospinal fluid. Spatial smoothing was applied using an 8 mm FWHM Gaussian kernel. Denoising involved linear regression including aCompCor (using the first five principal components from white matter and CSF masks), 12 realignment parameters (the six rigid-body motion parameters and their six first-order temporal derivatives), and ART-identified outlier regressors. The standard CONN denoising pipeline also applied band-pass filtering (0.008–0.09 Hz) and linear detrending[42].

We also conducted voxel-based morphometry (VBM) and, surface-based morphometry (SBM), using CAT12 (http://www.neuro.uni-jena.de/cat/) within SPM12 (http://www.fil.ion.ucl.ac.uk/spm/software/spm12). Moreover tract-based spatial statistics (TBSS) analyses were performed using the FMRIB Software Library (FSL6.0.7). VBM and SBM preprocessing were performed using CAT12 default settings, including tissue segmentation, spatial normalization, modulation, smoothing (8 mm FWHM for VBM), and default surface-based pipelines for SBM. Group comparisons were conducted using one-way ANOVA with age and sex as covariates (and total intracranial volume for VBM). TBSS analyses followed the standard FSL pipeline with default parameters (eddy-current and motion correction, brain extraction, tensor fitting, skeletonization), with voxel-wise group comparisons performed using permutation-based nonparametric testing (5000 permutations) and threshold-free cluster enhancement with family-wise error correction at $p < 0.05$.

ROI mask description

To examine rs-fMRI functional connectivity differences in PDICD+ patients compared to PDICD- and HC, we performed a ROI-to-ROI analysis focusing on the SN and CEN. All anatomical masks were obtained from the CONN toolbox and are based on network templates from the Human Connectome Project atlas[42,43]. The SN included the ACC, bilateral AI (AInsula), bilateral rostral prefrontal cortex (RPFC), and bilateral supramarginal gyrus (SMG). The CEN comprised the bilateral lateral prefrontal cortex (LPFC) and bilateral posterior parietal cortex (PPC). In total, 11 ROIs were included. Functional connectivity was assessed both within and between these networks to evaluate large-scale network interactions.

The 11 ROIs from SN and CEN were used for both ROI-to-ROI and seed-to-voxel analyses. For seed-to-voxel analysis, three additional ROIs previously implicated by our group in serotonergic dysfunction in PD patients with ICDs were included: the SMA, precentral gyrus, and right dorsolateral prefrontal cortex (dlPFC). These regions, where PDICD+ patients showed increased cortical 18F-altanserin binding in a previous study by our group[28], correspond to sensorimotor and associative networks involved in behavioral inhibition. These ROIs were defined using the Harvard-Oxford Atlas[82] as implemented in CONN.

First-level ROI-to-ROI analysis

The signal was averaged across voxels within each mask, resulting in one time course per ROI. Pearson's r correlation values between time courses were then computed for each pair of ROIs and Fisher-transformed. These values are referred to as resting-state functional connectivity (rsFC).

Second-level ROI-to-ROI group analysis

Second-level analyses were performed using a General Linear Model (GLM) framework implemented in the CONN toolbox[83]. Three groups were modeled as separate regressors, allowing both omnibus group effects (one-way ANOVA) and targeted pairwise comparisons. Specific between-group contrasts (e.g., PDICD+ vs. PDICD-, PDICD- vs. HC, PDICD+ vs. HC) were evaluated using t-contrasts within the same GLM, with residual variance estimated across all subjects. Covariates of no interest (gender, age) were included in all models; for PD group comparisons, MDS-UPDRS-III scores were also entered as covariate. Random-effects analyses were applied to account for inter-subject variability and the covariance structure across multiple measurements.

Inference was conducted at the level of connection clusters, defined as sets of functionally related ROI-to-ROI links. Cluster-level significance was assessed using parametric statistics on both within- and between-network connectivity (Functional Network Connectivity). Networks were delineated using complete-linkage hierarchical clustering based on anatomical proximity and functional similarity of ROI-to-ROI connectivity profiles. Statistical thresholds were set at a connection-level $p < 0.05$, with false discovery rate (FDR) correction applied at the cluster level (p-FDR < 0.05)[42,83].

Seed-based functional connectivity analysis

Seed-to-voxel analyses were conducted using the ROIs described above (11 SN and CEN ROIs plus the three serotonergic-related ROIs). For each seed, the average time series was extracted and correlated with the time series of every brain voxel, enabling whole-brain analyses of functional connectivity. Between-group comparisons were performed using two-sample t-tests, including gender and age as covariates, and MDS-UPDRS-III scores for PD groups. Statistical maps were thresholded at a voxel-wise level of $p < 0.005$ (uncorrected), followed by cluster-level FDR correction to identify significant regions of different functional connectivity between groups (p-FDR < 0.05).

Correlation and Path Analysis

Given the role of SN and CEN in ICDs in PD, we hypothesized that functional connectivity alterations would correlate with ICD severity and impulsivity measures. Relationships between functional connectivity measures and clinical/behavioral variables (QUIP-RS, UPPS, Kirby questionnaire to evaluate individual propensity to delay-discounting) were examined using Pearson or Spearman correlation coefficients.

Based on previous findings of altered serotonergic binding in the SMA, precentral gyrus, and right dlPFC in PDICD+ patients[28], we tested whether functional connectivity from these regions differed between groups. For regions showing significant group differences, we examined whether PET and rs-fMRI measures were associated with ICD severity. When both measures showed an association, we tested their direct contribution to ICD severity as well as their indirect effects through delay discounting behavior (Kirby questionnaire) or trait impulsivity measured by the UPPS. These associations were evaluated using structural equation modeling (SEM) with the lavaan package[84] in R. SEM allowed simultaneous estimation of bidirectional correlations between PET and connectivity, as well as direct paths from PET, connectivity, and behavioral measures to QUIP-RS scores. Models were estimated using maximum likelihood, and all variables were standardized prior to analysis.

Data availability

De-identified individual participant clinical and imaging data supporting the findings of the study are available on reasonable request to *bona fide* researchers, after approval of a research proposal by the corresponding authors. Code availability. The code used in this study are available on request from the corresponding authors.

Code availability

The code used in this study are available on request from the corresponding authors.

Received: 3 November 2025; Accepted: 8 February 2026;
Published online: 26 February 2026

References

1. Weintraub, D. & Claassen, D. O. Impulse control and related disorders in Parkinson's disease. *Int. Rev. Neurobiol.* **133**, 679–717 (2017).
2. Kelly, M. J., Baig, F., Hu, M. T. M. & Okai, D. Spectrum of impulse control behaviours in Parkinson's disease: Pathophysiology and management. *J. Neurol. Neurosurg. Psychiatry* **91**, 703–711 (2020).
3. Corvol, J. C. et al. Longitudinal analysis of impulse control disorders in Parkinson disease. *Neurology* **91**, e189–e201 (2018).
4. Marques, A. & Lewis, S. Impulse control disorders in Parkinson's disease: what's new? *J. Neurol.* **272**, 138 (2025).
5. Debove, I. et al. Management of impulse control and related disorders in Parkinson's disease: an expert consensus. *Movement Dis.* **39**, 235–248 (2024).
6. Terenzi, D. et al. Effects of tDCS on reward responsiveness and valuation in Parkinson's patients with impulse control disorders. *J. Neurol.* https://doi.org/10.1007/s00415-021-10733-0 (2021).
7. Rabinak, C. A. & Nirenberg, M. J. Dopamine agonist withdrawal syndrome in parkinson disease. *Arch. Neurol.* **67**, 58–63 (2010).
8. Bastiaens, J., Dorfman, B. J., Christos, P. J. & Nirenberg, M. J. Prospective cohort study of impulse control disorders in Parkinson's disease. *Mov Disord* **28**, 327–333 (2013).
9. Terenzi, D. et al. Reward sensitivity in Parkinson's patients with binge eating. *Parkinsonism and Related Disorders* https://doi.org/10.1016/j.parkreldis.2018.03.007 (2018).
10. Okai, D. et al. Trial of CBT for impulse control behaviors affecting Parkinson patients and their caregivers. *Neurology* **80**, 792–799 (2013).
11. Weintraub, D., David, A. S., Evans, A. H., Grant, J. E. & Stacy, M. Clinical spectrum of impulse control disorders in Parkinson's disease. *Mov Disord* **30**, 121–127 (2015).
12. Zhang, J.-F. et al. Impulse control disorders in Parkinson's disease: epidemiology, pathogenesis and therapeutic strategies. *Front. Psychiatry* **12**, 635494 (2021).
13. Voon, V. et al. Impulsive choice and response in dopamine agonist-related impulse control behaviors. *Psychopharmacology* **207**, 645–659 (2010).
14. Voon, V. et al. Impulse control disorders and levodopa-induced dyskinesias in Parkinson's disease: an update. *Lancet Neurol.* **16**, 238–250 (2017).
15. Prange, S. & Thobois, S. Imaging of impulse control disorders in Parkinson's disease. *Revue Neurologique* **180**, 1078–1086 (2024).
16. Waskowiak, P., Koppelmans, V. & Ruitenberg, M. F. L. Trait anxiety as a risk factor for impulse control disorders in de novo Parkinson's disease. *J. Parkinson's Dis.* **12**, 689–697 (2022).
17. Carbone, F. & Djamshidian, A. Impulse control disorders in Parkinson's disease: an overview of risk factors, pathogenesis and pharmacological management. *CNS Drugs* **38**, 443–457 (2024).
18. Cormier, F., Muellner, J. & Corvol, J.-C. Genetics of impulse control disorders in Parkinson's disease. *J Neural Transm* **120**, 665–671 (2013).
19. Vallelunga, A. et al. Role of genetic polymorphisms of the dopaminergic system in Parkinson's disease patients with impulse control disorders. *Parkinsonism Relat. Disord.* **18**, 397–399 (2012).
20. Vriend, C. The neurobiology of impulse control disorders in Parkinson's disease: from neurotransmitters to neural networks. *Cell Tissue Res.* **373**, 327–336 (2018).
21. Napier, T. C. et al. Linking neuroscience with modern concepts of impulse control disorders in Parkinson's disease. *Movement Dis. Off. J. Movement Disorder Soc.* **30**, 141–149 (2015).
22. Biundo, R. et al. Patterns of cortical thickness associated with impulse control disorders in Parkinson's disease. *Movement Disorders* https://doi.org/10.1002/mds.26154 (2015).
23. Frosini, D. et al. Parkinson's Disease and pathological gambling: results from a functional MRI study. *Movement Disorders* **25**, 2449–2453 (2010).
24. Gu, L., Shu, H., Wang, Y. & Xu, H. Exploring brain changes of impulse control disorders in Parkinson's disease: an ALE study. *Front. Aging Neurosci.* **14**, 966525 (2022).
25. Baagil, H. et al. Neural correlates of impulse control behaviors in Parkinson's disease: analysis of multimodal imaging data. *NeuroImage: Clinical* **37**, 103315 (2023).
26. Cilia, R. et al. Pathological gambling in patients with Parkinson's disease is associated with fronto-striatal disconnection: a path modeling analysis. *Movement Disorders* **26**, 225–233 (2011).
27. Theis, H. et al. Impulsive-compulsive behaviour in early Parkinson's disease is determined by apathy and dopamine receptor D3 polymorphism. *npj Parkinson's Disease* **9**, 154 (2023).
28. Prange, S. et al. Serotonergic dysfunction in patients with impulse control disorders in Parkinson's disease. *Brain* **148**, 2108–2121 (2025).
29. Cilia, R. & Kaasinen, V. Overcoming the dopamine-centric model of impulse control disorders in Parkinson's disease: the role of 5-HT. *Brain* **148**, 1853–1856 (2025).
30. Cornblath, E. J., Lydon-Staley, D. M. & Bassett, D. S. Harnessing networks and machine learning in neuropsychiatric care. *Curr. Opin. Neurobiol.* **55**, 32–39 (2019).
31. Boes, A. D. et al. Network localization of neurological symptoms from focal brain lesions. *Brain* **138**, 3061–3075 (2015).
32. Bassett, D. S., Xia, C. H. & Satterthwaite, T. D. Understanding the emergence of neuropsychiatric disorders with network neuroscience. *Biol Psychiatry Cogn. Neurosci. Neuroimaging* **3**, 742–753 (2018).
33. Michalopoulou, P. G., Meshreky, K. M., Hommerich, Z. & Shergill, S. S. Neuromodulation and neural networks in psychiatric disorders: current status and emerging prospects. *Psychol. Med.* **55**, e281 (2025).
34. Nabizadeh, F. & Aarabi, M. H. Functional and structural lesion network mapping in neurological and psychiatric disorders: a systematic review. *Front. Neurol.* **14**, 1100067 (2023).
35. Gonzalez-Castillo, J., Kam, J. W. Y., Hoy, C. W. & Bandettini, P. A. How to interpret resting-state fMRI: ask your participants. *J. Neurosci.* **41**, 1130–1141 (2021).
36. Filip, P. et al. Disruption of multiple distinctive neural networks associated with impulse control disorder in Parkinson's disease. *Front. Hum. Neurosci.* **12**, 462 (2018).
37. Gu, L., Shu, H., Wang, Y. & Xu, H. Exploring brain changes of impulse control disorders in Parkinson's disease: an ALE study. *Front Aging Neurosci* **14**, 966525 (2022).
38. Tessitore, A. et al. Resting-state brain networks in patients with Parkinson's disease and impulse control disorders. *Cortex* **94**, 63–72 (2017).
39. Tessitore, A. et al. Intrinsic brain connectivity predicts impulse control disorders in patients with Parkinson's disease. *Movement Disord.* **32**, 1710–1719 (2017).
40. Carriere, N., Lopes, R., Defebvre, L., Delmaire, C. & Dujardin, K. Impaired corticostriatal connectivity in impulse control disorders in Parkinson disease. *Neurology* **84**, 2116–2123 (2015).
41. Navalpotro-Gomez, I. et al. Disrupted salience network dynamics in Parkinson's disease patients with impulse control disorders. *Parkinsonism Rel. Disord.* **70**, 74–81 (2020).

42. Whitfield-Gabrieli, S. & Nieto-Castanon, A. Conn: a functional connectivity toolbox for correlated and anticorrelated brain networks. *Brain Connect* **2**, 125–141 (2012).
43. Smith, S. M. et al. Correspondence of the brain's functional architecture during activation and rest. *Proc. Natl. Acad. Sci. USA* **106**, 13040–13045 (2009).
44. Yang, H. et al. Neural network localization in Parkinson's disease with impulse control disorders. *Front. Aging Neurosci.* **17**, 1549589 (2025).
45. Buckner, R. L., Andrews-Hanna, J. R. & Schacter, D. L. The brain's default network. *Ann. New York Acad. Sci.* **1124**, 1–38 (2008).
46. Dixon, M. L. et al. Heterogeneity within the frontoparietal control network and its relationship to the default and dorsal attention networks. *Proc. Natl. Acad. Sci USA* **115**, E1598–E1607 (2018).
47. Schaefer, A. et al. Local-global parcellation of the human cerebral cortex from intrinsic functional connectivity MRI. *Cereb Cortex* **28**, 3095–3114 (2018).
48. Glasser, M. F. et al. A multi-modal parcellation of human cerebral cortex. *Nature* **536**, 171–178 (2016).
49. Leech, R., Kamourieh, S., Beckmann, C. F. & Sharp, D. J. Fractionating the default mode network: distinct contributions of the ventral and dorsal posterior cingulate cortex to cognitive control. *J. Neurosci.* **31**, 3217–3224 (2011).
50. Housden, C. R., O'Sullivan, S. S., Joyce, E. M., Lees, A. J. & Roiser, J. P. Intact reward learning but elevated delay discounting in Parkinson's disease patients with impulsive-compulsive spectrum behaviors. *Neuropsychopharmacology* **35**, 2155–2164 (2010).
51. Martini, A., Lago, D. D., Edelstyn, N. M. J., Grange, J. A. & Tamburin, S. Impulse control disorder in parkinson's disease: A meta-analysis of cognitive, affective, and motivational correlates. *Front. Neurol.* https://doi.org/10.3389/fneur.2018.00654 (2018).
52. Pennisi, P. et al. Delay discounting in Parkinson's disease: a systematic review and meta-analysis. *Behav. Brain Res.* **436**, 114101 (2023).
53. Meyer, G. M. et al. Inhibitory control dysfunction in Parkinsonian impulse control disorders. *Brain* **143**, 3734–3747 (2020).
54. Girard, R. et al. Wait and you shall see: sexual delay discounting in hypersexual Parkinson's disease. *Brain* https://doi.org/10.1093/brain/awy298 (2019).
55. Dalley, J. W. & Robbins, T. W. Fractionating impulsivity: neuropsychiatric implications. *Nat Rev Neurosci* **18**, 158–171 (2017).
56. Voon, V., Mehta, A. R. & Hallett, M. Impulse control disorders in Parkinson's disease: recent advances. *Curr. Opin. Neurol.* **24**, 324–330 (2011).
57. Haber, S. N. & Knutson, B. The reward circuit: linking primate anatomy and human imaging. *Neuropsychopharmacology* **35**, 4–26 (2010).
58. Corbetta, M., Patel, G. & Shulman, G. L. The reorienting system of the human brain: from environment to theory of mind. *Neuron* **58**, 306–324 (2008).
59. Bernard, F. et al. The ventral attention network: the mirror of the language network in the right brain hemisphere. *J. Anat.* **237**, 632–642 (2020).
60. Luijten, M., Schellekens, A. F., Kühn, S., Machielse, M. W. J. & Sescousse, G. Disruption of reward processing in addiction: an image-based meta-analysis of functional magnetic resonance imaging studies. *JAMA Psychiatry* **74**, 387–398 (2017).
61. Mata-Marín, D. et al. A circuit-based approach to modulate hypersexuality in Parkinson's disease. *Psychiatry Clin. Neurosci.* **77**, 223–232 (2023).
62. Rodigari, A. & Oliveri, M. Disrupting SMA activity modulates explicit and implicit emotional responses: an rTMS study. *Neurosci. Lett.* **579**, 30–34 (2014).
63. Battaglia, S., Nazzi, C., Fazio, C. D. & Borgomaneri, S. The role of pre-supplementary motor cortex in action control with emotional stimuli: a repetitive transcranial magnetic stimulation study. *Ann. N. Y. Acad. Sci.* **1536**, 151–166 (2024).
64. LeDoux, J. The emotional brain, fear, and the amygdala. *Cell Mol. Neurobiol.* **23**, 727–738 (2003).
65. Phelps, E. A., Lempert, K. M. & Sokol-Hessner, P. Emotion and decision making: multiple modulatory neural circuits. *Ann. Rev. Neurosci.* https://doi.org/10.1146/annurev-neuro-071013-014119 (2014).
66. Kohn, N. et al. Neural network of cognitive emotion regulation-An ALE meta-analysis and MACM analysis. *NeuroImage* **87**, 345–355 (2014).
67. Rieu, I. et al. International validation of a behavioral scale in Parkinson's disease without dementia. *Mov Disord* **30**, 705–713 (2015).
68. Goetz, C. G. et al. Movement disorder society-sponsored revision of the unified Parkinson's Disease rating scale (MDS-UPDRS): scale presentation and clinimetric testing results. *Movement Disord.* **23**, 2129–2170 (2008).
69. Weintraub, D. et al. Questionnaire for impulsive-compulsive disorders in Parkinson's disease-rating scale. *Movement Disord.* **27**, 242–247 (2012).
70. Billieux, J. et al. Validation of a short French version of the UPPS-P impulsive behavior scale. *Compr Psychiatry* **53**, 609–615 (2012).
71. Roussakis, A.-A., Lao–Kaim, N. P. & Piccini, P. Brain imaging and impulse control disorders in Parkinson's disease. *Curr. Neurol. Neurosci. Rep.* **19**, 67 (2019).
72. Starkstein, S. E. et al. Reliability, validity, and clinical correlates of apathy in Parkinson's disease. *J. Neuropsychiatry Clin. Neurosci.* **4**, 134–139 (1992).
73. Spielberger, C. D. Stress and Anxiety in Sports. in *Anxiety In Sports* (Taylor & Francis, 1990).
74. Beck, A. T., Steer, R. A. & Brown, G. K. Beck Depression Inventory-II (BDI-II). *for Beck Depression Inventory-II* (BDI, 1993).
75. Stiasny-Kolster, K. et al. The REM sleep behavior disorder screening questionnaire-a new diagnostic instrument. *Mov. Disord.* **22**, 2386–2393 (2007).
76. Kirby, K. N., Petry, N. M. & Bickel, W. K. Monetary Choice Questionnaire. https://doi.org/10.1037/t10044-000 (2012).
77. Verbruggen, F. et al. A consensus guide to capturing the ability to inhibit actions and impulsive behaviors in the stop-signal task. *eLife* **8**, e46323 (2019).
78. Terenzi, D. et al. Social context and drug cues modulate inhibitory control in cocaine addiction: involvement of the STN evidenced through functional MRI. *Mol. Psychiatry* https://doi.org/10.1038/s41380-024-02637-y (2024).
79. Worbe, Y., Savulich, G., Voon, V., Fernandez-Egea, E. & Robbins, T. W. Serotonin depletion induces 'waiting impulsivity' on the human four-choice serial reaction time task: cross-species translational significance. *Neuropsychopharmacology* **39**, 1519–1526 (2014).
80. Tisdall, M. D. et al. Volumetric navigators for prospective motion correction and selective reacquisition in neuroanatomical MRI. *Magn. Reson. Med.* **68**, 389–399 (2012).
81. Power, J. D., Barnes, K. A., Snyder, A. Z., Schlaggar, B. L. & Petersen, S. E. Spurious but systematic correlations in functional connectivity MRI networks arise from subject motion. *Neuroimage* **59**, 2142–2154 (2012).
82. Desikan, R. S. et al. An automated labeling system for subdividing the human cerebral cortex on MRI scans into gyral based regions of interest. *Neuroimage* **31**, 968–980 (2006).
83. Nieto-Castanon, A. *Handbook of Functional Connectivity Magnetic Resonance Imaging Methods in CONN*. *Handbook of functional connectivity Magnetic Resonance Imaging methods in CONN*. https://doi.org/10.56441/hilbertpress.2207.6598 (2020).
84. Rosseel, Y. Lavaan: an R package for structural equation modeling. *J. Stat. Softw.* **48**, 1–36 (2012).

Acknowledgements

We thank all study participants and their families, the Association France Parkinson and Fondation Neurodis. The authors gratefully thank the CERMEP imaging center staff for their helpful support. This study was

supported by Fondation Neurodis and Association France Parkinson. S.P. was supported by a research grant from the Fondation pour la Recherche Médicale (FRM-FDM 40482) and Humboldt fellowship of the Alexander von Humboldt foundation.

Author contributions

D.T. and E.M. contributed equally to this work. D.T., E.M., S.T., and S.P. conceived the study. D.T. and E.M. performed the data analysis, and E.M. contributed to data collection. D.T. wrote the initial draft of the manuscript. F.L., H.K., M.H., M.D.O., J.R., and L.T. reviewed the manuscript and provided critical feedback. S.T. and S.P. supervised the project, secured funding, and contributed to manuscript revision. All authors reviewed and approved the final manuscript.

Competing interests

The authors declare no competing interests.

Additional information

Supplementary information The online version contains supplementary material available at https://doi.org/10.1038/s41531-026-01294-y.

Correspondence and requests for materials should be addressed to Damiano Terenzi or Stéphane Prange.